PROCEEDINGS OF SCIENCE

Prospective study on observations of γ-ray sources using the HADAR experiment

Xiangli Qian,[a,*] **Huiying Sun**[a] **and Xu Wang**[a] **for the HADAR collaboration**

[a] *School of Intelligent Engineering, Shandong Management University, No.3500 Dingxiang Rd, Changqing District, Jinan, China*

E-mail: qianxl@sdmu.edu.cn, sunhy@sdmu.edu.cn, wangxu@sdmu.edu.cn

The High Altitude Detection of Astronomical Radiation (HADAR) experiment is a refracting terrestrial telescope array based on the atmospheric Cherenkov imaging technique. It is a hybrid array consisting of four water-lens telescopes and a surrounding scintillation detector array for observing Cherenkov light induced by cosmic rays and gamma rays in the atmosphere from 10 GeV to 10 TeV . The HADAR experiment possesses the advantages of a large field-of-view and low energy threshold, so it can continuously scan large sky area and easily observe the galactic and extragalactic gamma-ray sources. In this study, we will present the prospects of using the HADAR experiment for the sky survey of gamma-ray sources based on Fermi-LAT sources, and provides a one-year operation of statistical significance. Through simulated analyses of these sources, it is anticipated that HADAR will detect a total of 93 gamma-ray sources with a significance exceeding 5 standard deviations during one year of operation. These sources comprise 45 galactic sources, 39 extragalactic sources, 3 sources of unknown type, and 6 unassociated sources.

38th International Cosmic Ray Conference (ICRC2023)
26 July - 3 August, 2023
Nagoya, Japan

*Speaker

PoS(ICRC2023)943

1. Introduction

Very high-energy (VHE) gamma rays (E $\geqslant$ 30 GeV), play a crucial role in investigating the production and acceleration of cosmic rays. Detecting VHE gamma rays stemming from non-thermal radiation processes and identifying their sources becomes a primary avenue for exploring cosmic structures and their electromagnetic components.

In the past two decades, more than 270 different types of VHE gamma-ray sources have been detected. VHE gamma-ray sources originate from diverse cosmic ray sources. Within our Galaxy, the emission mainly originates from supernova remnants (SNR), pulsar wind nebulae (PWNe), pulsars (PSR), binaries, and others. Outside the galaxy primarily arise from the radiation generated by Active Galactic Nuclei (AGN). AGN includes various categories, including blazars, blazar candidates of uncertain type (BCUs), radio galaxies (RDGs), quasars, and Seyfert galaxies (SEY), with blazars being the most prevalent among them. Blazars are an extremely active subtype of AGN that produce gamma-ray radiation through relativistic jets characterized by large Lorentz factors ($\geqslant$10). Over the past few decades, high-energy (E>100 MeV) gamma-ray radiation of blazars have been successfully detected through sky surveys conducted by the Energetic Gamma Ray Experiment Telescope (EGRET) and Fermi-LAT experiment.

However, space telescopes such as Fermi-LAT are not suitable for observing gamma rays with energies higher than 100 GeV due to their limited effective area ($\sim$1 m^2). Observations of VHE gamma rays are primarily conducted through IACTs and EAS experiments. IACTs have a large effective area ($\sim 10^5$ m^2), excellent angular and energy resolution, making them advantageous for studying gamma-ray sources with rapid variations. However, IACTs have a relatively small field-of-view (FOV) ($\sim$3.5–5°) and a low duty cycle (< 10 %), which restricts them to observe multiple sources simultaneously and trace the transient sources rapidly. On the other hand, EAS experiments have a wider FOV, enabling continuous observations of sources. However, they often have higher energy thresholds (hundreds of GeV) and poorer angular resolution. To overcome these limitations, a ground-based telescope experiment array called High Altitude Detection of Astronomical Radiation (HADAR) has been proposed. HADAR, independently developed by Chinese researchers, is an array of imaging atmospheric Cherenkov telescopes that employ refractive lenses to focus the atmospheric Cherenkov light generated by cosmic rays and gamma rays. Its primary objective is to detect gamma-ray radiation spanning from 10 GeV to 10 TeV using a wide FOV and lower energy thresholds.

HADAR enables continuous scanning and high-sensitivity observations of various celestial sources within its field, including point sources, transient sources, and variable sources. This research employs simulation based on Fermi-LAT data to explore the expected observations of both extragalactic and galactic gamma-ray sources by HADAR.

2. HADAR experiment

The HADAR experiment is a composite array consisting of wide-angle Cherenkov lens and scintillation detectors. The array structure is depicted in Figure 1(a). Its main goal is to detect and distinguish gamma rays by capturing the Cherenkov light emitted from cosmic rays and gamma rays. Figure 1(b) illustrates the structure of a single len, also referred to as a water-lens. Unlike IACTs that

utilize reflective lenses, HADAR utilizes an innovative water-refractive lens to overcome limitations of narrow FOV. The entire system comprises a refractive lens, water medium, light focusing system, and cylindrical tank. The FOV can reach up to 60°. For more details of the HADAR experiment, please refer to the literatures [1–3].

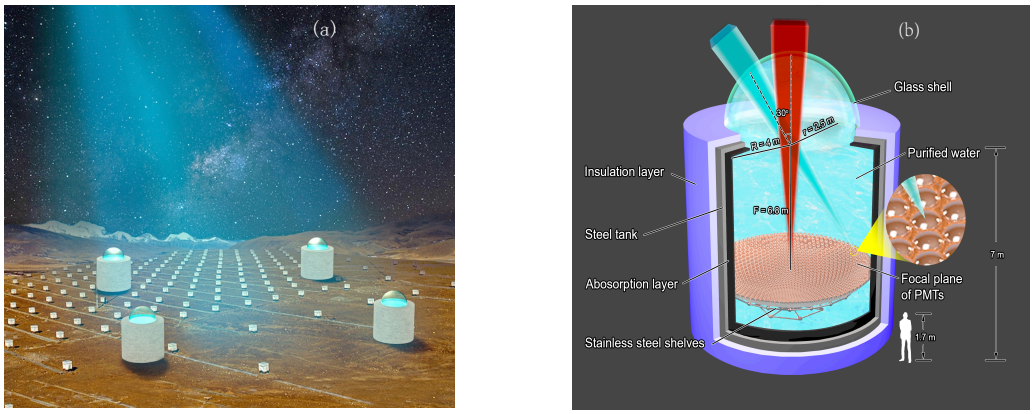

Figure 1: Schematic of HADAR: (a) Layout of the HADAR experiment; (b) Detailed design of a water-lens telescope[1].

The performance of the HADAR experiment, including effective area, angular resolution, and time resolution, can be found in references[1–3]. Figure 2 illustrates the sensitivity between HADAR and other experiments such as Fermi, MAGIC, H.E.S.S., ARGO-YBJ, HAWC, Tibet-ASγ, LHAASO, and CTA. The exposure time for IACT experiments is 50 h, while for EAS experiments, it is one year. From the figure, it is evident that HADAR can fill the energy gap left between ground-based and satellite experiments. The sensitivity of HADAR at 1 TeV is approximately 1% of the Crab Nebula flux[2]. Benefits from wide FOV, HADAR is advantageous for continuous observations of point sources and transient sources.

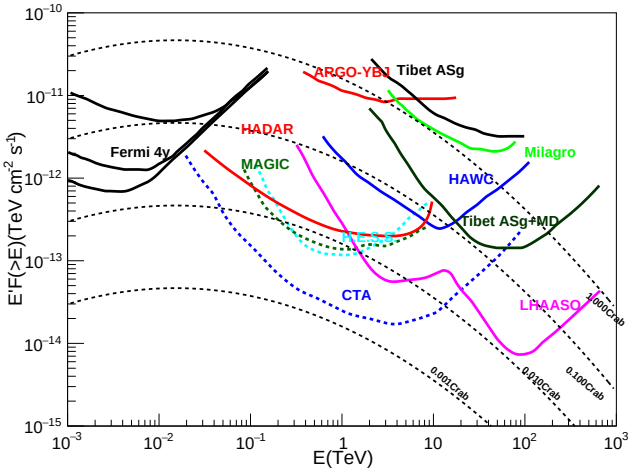

Figure 2: Comparisons of the sensitivity of HADAR with other γ-ray instruments[3].

3. Extrapolate the Fermi-LAT spectrum

In 2022, the Fermi-LAT collaboration issued the latest source catalog, 4FGL-DR3[4], alongside the fourth catalog dedicated to AGN, 4LAC-DR3[5]. The 4FGL-DR3 catalog contains 6,658 sources with a confidence level of 4σ or higher, encompassing both Galactic and extragalactic sources. The 6,658 sources are categorized into 27 classes, with AGN (4LAC-DR3) accounting for 3,814 sources including 9 subclasses. These subclasses comprise 792 FSRQs, 1,458 BL Lacs, 1,493 BCUs, and 71 non-blazar AGNs (including 6 subclasses).

Fermi-LAT data mainly cover the low-energy range, while HADAR extends its observations energy up to 10 TeV. Consequently, extrapolating the energy spectrum to VHE becomes necessary. During the process of VHE gamma-ray generation and propagation from the source to Earth, these gamma rays traverse the Extragalactic Background Light (EBL) radiation field and interact with EBL photons, producing electron-positron pairs, i.e., $\gamma_{\rm VHE}+\gamma_{\rm EBL} \rightarrow e^{+}+e^{-}$. This interaction leads to attenuation of the observed gamma-ray energy spectrum. The absorption effect is relatively weak in the low-energy range (<50 GeV) which is Fermi-LAT instrument primarily detects. Therefore, the energy spectra of Fermi-LAT gamma-ray sources can be considered as intrinsic spectra that without significant absorption. The absorption effect can be expressed by the formula:

$$(\frac{dN}{dE})_{obs} = (\frac{dN}{dE})_{int} \times e^{-\tau(E,z)}, \tag{1}$$

where $(\frac{dN}{dE})_{obs}$ represents the observed energy spectrum of gamma-ray sources, $(\frac{dN}{dE})_{int}$ corresponds to the intrinsic spectrum, and $e^{-\tau(E,z)}$ denotes the attenuation factor.

4. Expected spectra of the extragalactic sources

In this section, we apply energy extrapolation to the Fermi-LAT 4LAC-DR3 source. We selected sources within the HADAR FOV and with redshift values, resulting in a total of 992 sources (958 at high latitudes and 34 at low latitudes). It includes 492 BL Lacs, 376 FSRQs, 88 BCUs, and 36 Nonblazar AGNs. The extrapolated observed spectra are depicted in Figure 3, and the Domínguez model is adopted for the EBL. As a comparison, the HADAR sensitivity curve corresponding to one year of operation is demonstrated in order to evaluate the HADAR's observational capabilities. It shows that a portion of BL Lacs and Nonblazar AGN are the main classes, while rarely FSRQs and BCUs can be detected.

5. The expected observational significance of gamma-ray sources by HADAR

We performed a fast simulation to generate gamma-ray and cosmic ray events and adopted a sky scanning analysis method based on the equi-zenith angle to calculate the significance. For a detailed description of this method, please refer to references[2, 3, 6]. Here, we give a general description of the calculation steps:

(1) Estimate the observation time of HADAR accurately. Since HADAR can only collect Cherenkov light effectively on clear moonless nights, it is necessary to calculate the daily effective observation time for each source and accumulate it to obtain the total effective time for one year.

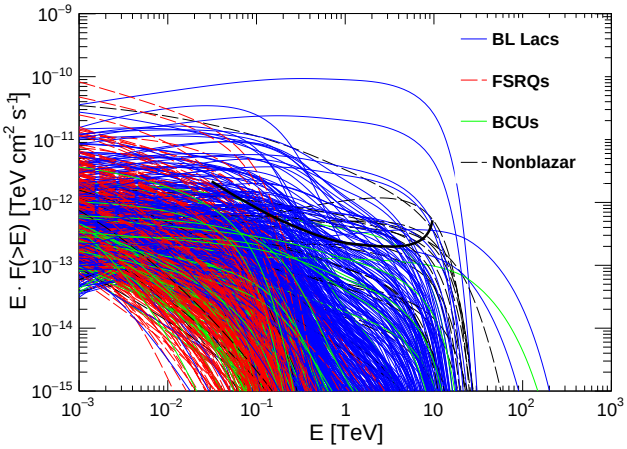

Figure 3: The expected energy spectrum for extragalactic sources.

(2) Setup celestial and horizon coordinate system and divide them into windows. The background events for the "on-source window" can be estimated as the average value of all events in the "off-source windows".

(3) Based on the energy spectra information of Fermi-LAT sources, calculate the excess of gamma-ray events to determine the statistical significance of the sources.

The simulation results show that for a one-year operation, HADAR is expected to detect 39 extragalactic gamma-ray sources with a significance over 5 standard deviations. Out of these 39 sources, 34 are BL Lacs, 2 are FSRQs (CTA 102 and 3C 454.3), and 3 are non-blazar AGNs (NGC 1275, M87, and B2 1447+27). No anticipated observation of starburst galaxies and normal galaxies. Within the Galaxy, HADAR is expected to observe 45 gamma-ray sources, including 34 pulsars, 10 pulsar wind nebulae and supernova remnants, and 1 stellar-forming region. Additionally, 3 sources of unknown type and 6 unassociated sources are anticipated to be observed. Detailed information for each source is provided in Tables 1 and 2, and the two-dimensional significance sky map is depicted in Figure 4.

6. Conclusion

The HADAR experiment introduces an innovative approach by utilizing pure water and hemispherical lens to construct large FOV Cherenkov telescope. This design offers several advantages, including low energy threshold, high sensitivity, and a large FOV, which is quite different from traditional IACTs. HADAR is an ideal detector for searching gamma-ray bursts and transient sources, as well as for all-sky gamma-ray sources scanning.

This study we conducted a detailed prospection of HADAR's observational capabilities by utilizing the latest Fermi-LAT 4FGL-DR3 and 4LAC-DR3 sources. Results show that HADAR, operating for one year, will observe a total of 93 gamma-ray sources with a significance level exceeding 5 standard deviations. It includes 45 Galactic sources, 39 extragalactic sources, 3 sources of unknown type, and 6 unassociated sources.

Table 1: A list of property parameters for extragalactic sources in HADAR FOV, where the spectral model parameters are derived from 4LAC-DR3. Columns from left to right are as follows: 4FGL source name, counterpart, right ascension, declination, class, redshift, model, E_0, differential flux at E_0 with the fit model, spectral index Γ, curvature parameter β, live time and significance.

4FGL Name	Counterpart	R.A.	Dec.	Type	Redshift	Model	E_0/ GeV	F_0/ $\mathrm{TeV^{-1}cm^{-2}s^{-1}}$	Γ	β	Time/ hrs	S/σ
J0112.1+2245	S2 0109+22	18.03	22.75	BLL	0.265	LP	0.769	1.46×10^{-5}	1.99	0.060	277.8	9.05
J0211.2+1051	MG1 J021114+1051	32.81	10.86	BLL	0.200	LP	0.922	7.51×10^{-6}	2.02	0.042	196.3	6.47
J0222.6+4302	3C 66A	35.67	43.04	BLL	0.444	LP	1.246	8.40×10^{-6}	1.89	0.046	264.2	17.9
J0319.8+4130	NGC 1275	49.96	41.51	RDG	0.018	LP	0.918	4.36×10^{-5}	2.05	0.069	271.9	54.6
J0521.7+2112	TXS 0518+211	80.44	21.21	bll	0.108	LP	1.541	4.64×10^{-6}	1.86	0.045	271.0	50.2
J0620.7+2643	RX J0620.6+2644	95.18	26.73	bll	0.134	PL	17.415	1.22×10^{-9}	1.55	0.000	290.3	5.1
J0648.7+1516	RX J0648.7+1516	102.19	15.28	bll	0.179	LP	3.248	1.22×10^{-7}	1.60	0.056	234.3	10.9
J0650.7+2503	1ES 0647+250	102.7	25.05	bll	0.203	LP	2.067	8.44×10^{-7}	1.65	0.041	286.0	32.9
J0738.1+1742	PKS 0735+17	114.54	17.71	bll	0.424	LP	1.623	2.25×10^{-6}	1.97	0.067	251.3	5.2
J0809.8+5218	1ES 0806+524	122.46	52.31	BLL	0.138	LP	1.342	1.91×10^{-6}	1.83	0.023	193.9	15.1
J0915.9+2933	Ton 0396	138.99	29.55	bll	0.190	LP	1.390	9.28×10^{-7}	1.74	0.081	294.7	7.4
J1015.0+4926	1H 1013+498	153.77	49.43	bll	0.212	LP	1.044	6.00×10^{-6}	1.75	0.044	220.0	27.9
J1058.6+5627	TXS 1055+567	164.67	56.46	BLL	0.143	LP	1.102	2.38×10^{-6}	1.86	0.050	149.4	6.1
J1104.4+3812	Mkn 421	166.12	38.21	BLL	0.030	PLEC	1.258	1.79×10^{-5}	1.74	0.000	284.9	519.6
J1117.0+2013	RBS 0958	169.27	20.23	bll	0.139	PL	1.964	3.12×10^{-7}	1.95	0.000	266.1	5.0
J1120.8+4212	RBS 0970	170.20	42.20	bll	0.124	LP	2.416	2.11×10^{-7}	1.55	0.046	268.6	23.9
J1150.6+4154	RBS 1040	177.66	41.91	bll	0.320	LP	1.949	4.71×10^{-7}	1.55	0.135	270.0	7.2
J1217.9+3007	B2 1215+30	184.48	30.12	BLL	0.130	LP	1.248	5.77×10^{-6}	1.87	0.043	295.1	37.7
J1221.3+3010	PG 1218+304	185.34	30.17	bll	0.184	LP	2.590	5.27×10^{-7}	1.65	0.029	295.2	37.4
J1221.5+2814	W Comae	185.38	28.24	bll	0.102	LP	0.781	6.00×10^{-6}	2.11	0.024	293.1	5.5
J1230.2+2517	ON 246	187.56	25.30	bll	0.135	LP	0.800	6.66×10^{-6}	2.02	0.056	286.7	5.8
J1230.8+1223	M 87	187.71	12.39	rdg	0.004	LP	1.124	1.30×10^{-6}	2.00	0.036	210.5	5.3
J1417.9+2543	1E 1415.6+2557	214.49	25.72	bll	0.237	LP	8.155	6.13×10^{-9}	1.28	0.138	287.9	5.1
J1427.0+2348	PKS 1424+240	216.76	23.80	BLL	0.604	LP	1.254	5.70×10^{-6}	1.71	0.057	281.8	21.7
J1428.5+4240	H 1426+428	217.13	42.68	bll	0.129	PL	5.135	2.69×10^{-8}	1.65	0.000	266.1	10.3
J1449.5+2746	B2 1447+27	222.40	27.77	rdg	0.031	PL	14.614	5.37×10^{-10}	1.46	0.000	292.4	6.8
J1555.7+1111	PG 1553+113	238.93	11.19	BLL	0.360	LP	3.802	1.16×10^{-6}	1.57	0.095	199.5	56.4
J1653.8+3945	Mkn 501	253.47	39.76	BLL	0.033	LP	1.508	3.78×10^{-6}	1.75	0.018	279.5	125.1
J1725.0+1152	1H 1720+117	261.27	11.87	bll	0.180	LP	2.216	7.55×10^{-7}	1.76	0.056	205.9	14.5
J1728.3+5013	I Zw 187	262.08	50.23	bll	0.055	PL	2.983	1.82×10^{-7}	1.79	0.000	213.2	21.1
J1838.8+4802	GB6 J1838+4802	279.71	48.04	bll	0.300	LP	1.631	8.39×10^{-7}	1.78	0.040	231.3	6.7
J1904.1+3627	MG2 J190411+3627	286.03	36.45	bll	0.078	PL	5.074	2.01×10^{-8}	1.80	0.000	289.7	5.8
J2116.2+3339	B2 2114+33	319.06	33.66	bll	0.350	LP	1.653	1.10×10^{-6}	1.75	0.095	294.4	7.1
J2202.7+4216	BL Lac	330.69	42.28	BLL	0.069	LP	0.871	4.07×10^{-5}	2.12	0.059	268.2	27.4
J2232.6+1143	CTA 102	338.15	11.73	FSRQ	1.037	PLEC	1.082	4.34×10^{-5}	2.27	0.000	204.5	5.9
J2250.0+3825	B3 2247+381	342.51	38.42	bll	0.119	PL	5.338	2.55×10^{-8}	1.74	0.000	284.2	7.9
J2253.9+1609	3C 454.3	343.50	16.15	FSRQ	0.859	PLEC	0.892	1.32×10^{-4}	2.38	0.000	240.7	10.9
J2323.8+4210	1ES 2321+419	350.97	42.18	bll	0.059	LP	1.857	5.31×10^{-7}	1.80	0.068	268.7	11.0
J2347.0+5141	1ES 2344+514	356.77	51.70	bll	0.044	LP	1.911	7.15×10^{-7}	1.74	0.039	199.8	29.2

Table 2: A list of property parameters for galactic sources in HADAR FOV, where the spectral model parameters are derived from 4FGL-DR3.

4FGL Name	Counterpart	R.A.	Dec.	Type	Model	E_0/ GeV	F_0/ $\mathrm{TeV^{-1}cm^{-2}s^{-1}}$	Γ	β	Time/ hrs	S/σ
J0030.4+0451	PSR J0030+0451	7.61	4.86	MSP	PLEC	1.360	7.36×10^{-6}	2.08	0.000	130.1	40.6
J0102.8+4839	PSR J0102+4839	15.71	48.66	MSP	PLEC	1.378	1.42×10^{-6}	2.18	0.000	226.4	6.0
J0106.4+4855	PSR J0106+4855	16.61	48.93	PSR	PLEC	1.578	1.66×10^{-6}	2.11	0.000	224.2	14.2
J0218.1+4232	PSR J0218+4232	34.53	42.55	MSP	PLEC	0.820	1.20×10^{-5}	2.35	0.000	266.8	6.2
J0220.1+1155	-	35.04	11.92	-	PL	16.622	3.98×10^{-10}	1.57	0.000	206.2	5.6
J0340.3+4130	PSR J0340+4130	55.10	41.51	MSP	PLEC	1.659	1.38×10^{-6}	2.03	0.000	271.9	24.6
J0357.8+3204	PSR J0357+3205	59.46	32.08	PSR	PLEC	1.104	1.26×10^{-5}	2.30	0.000	295.5	19.3
J0425.6+5522e	SNR G150.3+04.5	66.42	55.37	SNR	LP	7.240	1.19×10^{-7}	1.64	0.047	161.8	123.6
J0534.5+2201i	Crab Nebula	83.63	22.02	PWN	LP	10.000	5.50×10^{-7}	1.75	0.080	274.7	639.6
J0540.3+2756e	Sim 147	85.10	27.94	SNR	LP	1.192	5.50×10^{-6}	2.07	0.081	292.7	11.1
J0554.1+3107	PSR J0554+3107	88.55	31.12	PSR	PLEC	1.066	4.06×10^{-6}	2.34	0.000	295.5	5.1
J0605.1+3757	PSR J0605+3757	91.28	37.96	MSP	PLEC	1.507	7.88×10^{-7}	2.18	0.000	285.7	5.3
J0617.2+2234e	IC 443	94.31	22.58	SNR	LP	4.551	2.58×10^{-6}	2.28	0.123	277.1	37.6
J0620.9+2201	-	95.23	22.02	-	PL	20.913	6.45×10^{-10}	1.61	0.000	274.7	5.7
J0631.5+1036	PSR J0631+1036	97.88	10.60	PSR	PLEC	1.540	2.52×10^{-6}	2.20	0.000	193.8	11.1
J0631.8+0645	PSR J0631+0646	97.96	6.76	PSR	PLEC	2.258	7.60×10^{-7}	2.22	0.000	152.9	5.9
J0633.7+0632	PSR J0633+0632	98.44	6.54	PSR	PLEC	1.527	8.13×10^{-6}	2.22	0.000	150.4	26.3
J0633.9+1746	PSR J0633+1746	98.48	17.77	PSR	PLEC	1.670	3.19×10^{-4}	2.10	0.000	251.7	575.7
J0650.6+2055	NVSS J065035+205556	102.66	20.93	unk	LP	3.643	4.42×10^{-8}	1.63	0.096	269.6	9.5
J0751.2+1808	PSR J0751+1807	117.80	18.14	MSP	PLEC	1.643	9.45×10^{-7}	2.06	0.000	254.1	13.1
J1312.7+0050	PSR J1312+0051	198.19	0.84	MSP	PLEC	1.301	2.01×10^{-6}	2.15	0.000	76.3	5.7
J1554.2+2008	-	238.55	20.15	-	PL	4.619	1.14×10^{-8}	1.82	0.000	265.6	5.0
J1816.5+4510	PSR J1816+4510	274.15	45.17	MSP	PLEC	1.171	1.48×10^{-6}	2.14	0.000	251.6	6.1
J1836.2+5925	PSR J1836+5925	279.06	59.43	PSR	PLEC	1.428	6.64×10^{-5}	2.07	0.000	112.6	388.8
J1846.3+0919	PSR J1846+0919	281.60	9.33	PSR	PLEC	1.458	3.78×10^{-6}	2.19	0.000	181.0	14.9
J1854.5+2050	-	283.64	20.84	-	PL	103.233	2.68×10^{-11}	1.01	0.000	269.2	34.8
J1857.7+0246e	HESS J1857+026	284.45	2.77	PWN	PL	6.063	2.25×10^{-7}	2.13	0.000	103.1	19.5
J1907.9+0602	PSR J1907+0602	286.98	6.04	PSR	PLEC	1.898	1.39×10^{-5}	2.37	0.000	144.4	31.3
J1910.8+2856	NVSS J191052+285621	287.72	28.94	unk	PL	7.243	6.08×10^{-9}	1.80	0.000	294.1	7.1
J1911.0+0905	W 49B	287.76	9.09	snr	LP	4.552	7.74×10^{-7}	2.28	0.112	178.6	8.5
J1918.0+0331	NVSS J191803+033032	289.51	3.52	unk	PL	12.647	2.39×10^{-9}	1.72	0.000	113.0	6.2
J1923.2+1408e	W 51C	290.82	14.14	SNR	LP	2.768	5.08×10^{-6}	2.21	0.109	225.4	25.9
J1924.3+1628	-	291.10	16.48	-	PL	22.893	7.99×10^{-10}	1.76	0.000	243.1	7.7
J1952.9+3252	PSR J1952+3252	298.25	32.88	PSR	PLEC	1.618	9.92×10^{-6}	2.29	0.000	295.1	39.3
J1954.3+2836	PSR J1954+2836	298.59	28.60	PSR	PLEC	1.519	8.08×10^{-6}	2.32	0.000	293.7	23.1
J1958.7+2846	PSR J1958+2846	299.68	28.77	PSR	PLEC	1.356	1.13×10^{-5}	2.35	0.000	293.9	21.1
J2017.4+0602	PSR J2017+0603	304.35	6.05	MSP	PLEC	1.800	2.20×10^{-6}	1.98	0.000	144.6	43.2
J2017.9+3625	PSR J2017+3625	304.49	36.43	PSR	PLEC	1.467	6.99×10^{-6}	2.53	0.000	289.8	5.7
J2021.0+4031e	gamma Cygni	305.27	40.52	SNR	LP	7.758	2.07×10^{-7}	1.88	0.060	276.4	95.9
J2021.1+3651	PSR J2021+3651	305.28	36.86	PSR	PLEC	1.842	2.62×10^{-5}	2.32	0.000	288.8	114.0
J2028.3+3331	PSR J2028+3332	307.08	33.53	PSR	PLEC	1.467	6.57×10^{-6}	2.32	0.000	294.6	17.5
J2028.6+4110e	Cygnus X	307.17	41.17	SFR	LP	2.036	2.90×10^{-5}	2.04	0.033	273.5	368.3
J2030.0+3641	PSR J2030+3641	307.51	36.69	PSR	PLEC	1.650	3.92×10^{-6}	2.33	0.000	289.2	12.6
J2030.9+4416	PSR J2030+4415	307.73	44.27	PSR	PLEC	1.284	6.77×10^{-6}	2.47	0.000	257.2	5.4
J2032.2+4127	PSR J2032+4127	308.06	41.46	PSR	PLEC	2.918	3.31×10^{-6}	2.26	0.000	272.2	47.2
J2035.0+3632	PSR J2034+3632	308.76	36.54	MSP	PLEC	2.456	5.99×10^{-7}	2.17	0.000	289.5	11.3
J2043.3+1711	PSR J2043+1711	310.84	17.19	MSP	PLEC	1.222	3.47×10^{-6}	2.10	0.000	247.9	20.9
J2055.8+2540	PSR J2055+2539	313.96	25.67	PSR	PLEC	1.279	8.39×10^{-6}	2.18	0.000	287.7	26.6
J2111.4+4606	PSR J2111+4606	317.86	46.10	PSR	PLEC	1.305	4.84×10^{-6}	2.26	0.000	245.4	11.9
J2214.6+3000	PSR J2214+3000	333.67	30.01	MSP	PLEC	1.090	5.97×10^{-6}	2.06	0.000	295.1	28.8
J2301.9+5855e	CTB 109	345.49	58.92	SNR	LP	3.461	1.57×10^{-7}	1.91	0.054	119.2	6.8
J2302.7+4443	PSR J2302+4442	345.69	44.72	MSP	PLEC	2.049	2.04×10^{-6}	2.02	0.000	254.5	55.8
J2304.0+5406e	-	346.01	54.11	-	LP	14.034	1.58×10^{-8}	1.76	0.127	175.6	18.0
J2323.4+5849	Cas A	350.86	58.82	snr	LP	2.232	1.38×10^{-6}	1.87	0.076	120.5	20.9

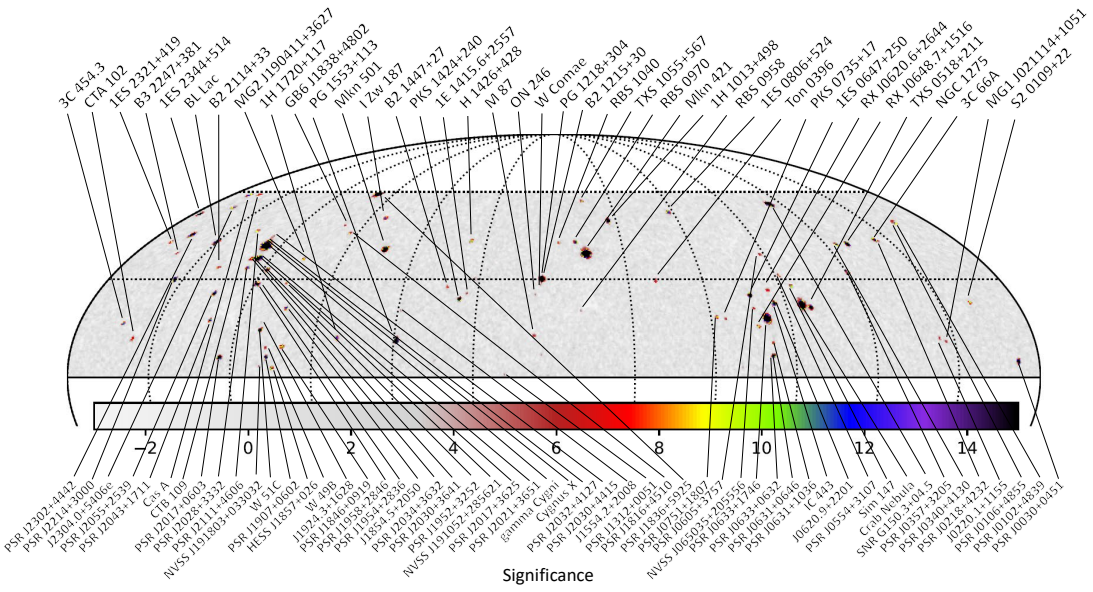

Figure 4: Expected significance sky map of HADAR observations with respect to Fermi-LAT sources in the equatorial coordinates (J2000 epoch). The map is annotated with extragalactic sources (up) and galactic sources, unknown sources, and unassociated sources (down).

References

[1] G. G. Xin, Y. H. Yao, X. L. Qian, *Prospects for the Detection of the Prompt Very-high-energy Emission from γ-ray Bursts with the High Altitude Detection of Astronomical Radiation Experiment*, *Astrophys. J.* **923** 112

[2] X. L. Qian, H. Y. Sun, T. L. Chen, *Prospective study on observations of γ-ray sources in the Galaxy using the HADAR experiment*, *Front. Phys-Beijing* **17** 64602

[3] X. L. Qian, H. Y. Sun, T. L. Chen, *Prospective study on observations of gamma-ray emission from active galactic nuclei using the HADAR experiment (in chinese)*, *Acta Phys. Sin.* **72** 049501

[4] S. Abdollahi, F. Acero, L. Baldini, *Incremental fermi large area telescope fourth source catalog*, *Astrophys. J. Suppl. S.* **260** 53

[5] M. Ajello, L. Baldini, J. Ballet, *The Fourth Catalog of Active Galactic Nuclei Detected by the Fermi Large Area Telescope: Data Release 3*, *Astrophys. J. Suppl. S.* **263** 24

[6] M. Amenomori, S. Ayabe, D. Chen, *A Northern Sky Survey for Steady Tera-Electron Volt Gamma-Ray Point Sources Using the Tibet Air Shower Array*, *Astrophys. J.* **633** 1005